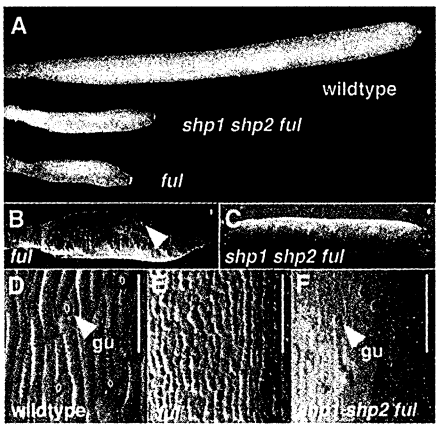

Fig. 3. Mutations in *SHP1* and *SHP2* partially suppress the valve differentiation defects of *ful* fruit and largely eliminate valve tearing. **(A)** Like *ful-1* fruit, *shp1 shp2 ful-1* fruit (stage 17) are much shorter than the wild type, due to the lack of valve expansion after fertilization. Valve tears (arrowhead) are present in nearly all *ful-1* fruit **(B)** and are rarely seen in *shp1 shp2 ful-1* fruit **(C)**. Guard cells (gu) are present in wild-type and *shp1 shp2 ful-1* fruit valves **(D** and **F)** and are not found in *ful-1* fruit valves **(E)**. Bars, 100 μm.

lutely required for GT140 expression in *ful* mutant valves, indicating that additional genes are involved in activating this marker.

The data presented here, together with other recently published observations, allow us to propose a model (Fig. 4) for some of the genetic interactions underlying valve margin development. The *SHP* genes are positively regulated by the *AGAMOUS* MADS-box gene product (*8*, *9*) and are required for proper valve margin development (*6*). Besides directing valve differentiation (*2*), FUL negatively regulates *SHP* expression, ensuring that valve margin cell fate occurs only at the valve boundary. Although not shown in the model, SHP1/2 may negatively regulate a replum-specific factor; expansion of such a factor's activity in *shp1 shp2* fruit could account for the observed slight restriction of *FUL* valve expression (Fig. 2, E and F). Expression of the GT140 valve margin marker is positively regulated by SHP1/2 (*6*) and negatively regulated by FUL, which may occur by way of an additional factor (factor X) involved in GT140 activation.

Fig. 4. Genetic interactions involved in valve margin development.

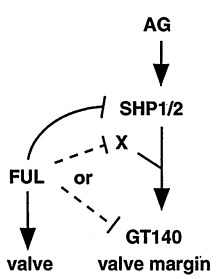

References and Notes

1. J. Spence, Y. Vercher, P. Gates, N. Harris, *J. Microsc.* **181**, 195 (1996).
2. Q. Gu, C. Ferrándiz, M. Yanofsky, R. Martienssen, *Development* **125**, 1509 (1998).
3. A. M. Mandel and M. F. Yanofsky, *Plant Cell* **7**, 1763 (1995).
4. P. N. Benfey and N. -H. Chua, *Science* **250**, 959 (1990).
5. The *FUL* cDNA was cloned into the pBIN-JIT vector, a pBIN19 (Clontech) derivative, which placed *FUL* transcription under the control of a tandem repeat of the 35S promoter. Eighteen of 28 independent transformants in the Columbia (Col) ecotype had similar phenotypes, and two lines (CFM5088 and CFM5092) were selected for further study. In addition to the phenotypes described, 35S::FUL plants flowered early, produced terminal flowers, and showed a threefold increase in seed weight.
6. S. J. Liljegren *et al.*, *Nature* **404**, 766 (2000).
7. Microscopy, tissue fixation, and histology were as described (*2*, *6*). Plastic sections (1 μm) are shown in Fig. 1, C and D, and paraplast sections (8 or 10 μm) are shown elsewhere.
8. B. Savidge, S. D. Rounsley, M. F. Yanofsky, *Plant Cell* **7**, 721 (1995).
9. C. A. Flanagan, Y. Hu, H. Ma, *Plant J.* **10**, 343 (1996).
10. RNA in situ hybridizations of wild-type (Col), *ful-2* (*15*), 35S::FUL, and *shp1-1 shp2-1* sections were done as described (*15*) with the *SHP1* (*9*), *SHP2* (*8*), and *FUL* (*3*) probes. 35S::SHP1/2 plants (*6*) were crossed to *ful-1* mutants (*2*), because a β-glucuronidase (GUS)–containing enhancer trap element inserted in the 5′-untranslated region behaves as an accurate reporter of *FUL* expression in *ful-1*/+ plants. GUS assays of 35S::SHP1/2 *ful-1*/+ fruit were as described (*6*).
11. C. Ferrándiz, S. Liljegren, M. Yanofsky, data not shown.
12. *shp1 shp2 ful-1* and *shp1 shp2 ful-2* fruit were compared with *ful-1* and *ful-2* fruit, respectively. Fruit lengths (in millimeters; $n = 30$) at stage 18 were as follows: wild type (Landsberg *erecta*), 14.2 ± 0.4; *ful-1*, 3.9 ± 0.1; *shp1 shp2 ful-1*, 4.1 ± 0.2; wild type (Col), 16.5 ± 0.5; *ful-2*, 5.6 ± 0.5; *shp1 shp2 ful-2*, 7.2 ± 0.5. Valve tears were present in 91.0% of *ful-1*, 2.5% of *shp1 shp2 ful-1*, and 0% of wild-type fruit ($n \geq 79$, stages 17 to 19). Stomata were also observed in *shp1 shp2 ful-2* fruit valves.
13. V. Sundaresan *et al.*, *Genes Dev.* **9**, 1797 (1995).
14. Plants carrying the GT140 marker were crossed to *ful-2*, *shp1 shp2 ful-2*, and 35S::FUL plants, and GUS assays were as described (*6*).
15. C. Ferrándiz, Q. Gu, R. Martienssen, M. F. Yanofsky, *Development* **127**, 725 (2000).

16. We thank A. Chen, S. Guimil, T. Kawashiwa, T. Khammungkhune, T. Kuhlmann, and C. Wiley for technical assistance. Supported by grants from the National Science Foundation.

11 April 2000; accepted 26 May 2000

Interdigital Regulation of Digit Identity and Homeotic Transformation by Modulated BMP Signaling

Randall D. Dahn and John F. Fallon*

The developmental mechanisms specifying digital identity have attracted 30 years of intense interest, but still remain poorly understood. Here, through experiments on chick foot development, we show digital identity is not a fixed property of digital primordia. Rather, digital identity is specified by the interdigital mesoderm, demonstrating a patterning function for this tissue before its regression. More posterior interdigits specify more posterior digital identities, and each primordium will develop in accordance with the most posterior cues received. Furthermore, inhibition of interdigital bone morphogenetic protein (BMP) signaling can transform digit identity, suggesting a role for BMPs in this process.

Although the signaling pathways that broadly establish polarity along the three axes of the developing limb bud are rapidly being elucidated (*1*), the downstream mechanisms that exquisitely pattern adult morphology are not well understood. For instance, in the developing chick limb bud the posterior mesodermal zone of polarizing activity (ZPA) controls anteroposterior (A/P) polarity through expression of the *Sonic hedgehog* (*Shh*) gene (*2*). However, the mechanisms by which early asymmetry is translated into the characteristic differences in phalangeal number and morphology that define digital identity are not understood. Application of ectopic SHH protein (SHH-N) or ZPA cells to the anterior border of early-stage limb buds elicits mirror-image patterns of digit duplication in a dose- and time-dependent manner (*2*, *3*). A recent report suggests that in the early limb bud, SHH acts long range to control digit number and short range to establish a BMP2 morphogen gradient that specifies digit identity in a dose-dependent fashion by progressively promoting anterior digital precursors to more posterior identities (*4*). This hypothesis implies that A/P positional value is specified during early limb bud stages under direct SHH influence and, by the time digital rays are forming, A/P positional value is a fixed property of digital primordia. Here, we employ both embryological and molecular methodologies to demonstrate that the

Department of Anatomy, University of Wisconsin, 1300 University Avenue, Madison, WI 53706, USA.

*To whom correspondence should be addressed. E-mail: jffallon@facstaff.wisc.edu

developmental mechanisms specifying digital identity operate at autopodial stages. A/P identity is not a fixed property of digital primordia, but remains labile after primordia have formed. We further show that digital identity is specified by the interdigital (ID) mesoderm, through a mechanism requiring BMP signaling.

The chick foot is an ideal system in which to examine the regulation of digital identity, despite the current lack of molecular markers of identity; each digit of the chick foot is distinguishable by the number and morphology of phalanges and by overall length (Fig. 1A). We first examined the regulation of digital identity in developing chick leg buds by proximodistal bisection of digit 2 (d2) and digit 3 (d3) primordia (p2 and p3, respectively) with foil barriers (Fig. 1B). Primordia were bisected after the precartilaginous digital rays had condensed, but before the specification of interphalangeal joints as revealed by the absence of *Gdf5* expression, a molecular marker of presumptive joints (*5*). It is also worth noting that *Shh* expression in the leg bud is extinguished by St. $26^{+}/27^{-}$ (*6*), before the stages at which bisections were performed (*7*). In all cases, the posterior components of p2 (postp2) developed with three phalanges characteristic of normal d2 identity (Fig. 1C). In contrast, most p2 anterior components (antp2) underwent homeotic transformation [defined in (*8*)], developing with only two phalanges whose morphology is characteristic of the adjacent d1 (74%, $n = 27$). The transformation of antp2 identity occurs very rapidly; 48 hours after surgery, antp2 morphology and *Gdf5* expression (Fig. 1D) are comparable to that of d1 ($n = 6$). Similar results were obtained from p3 bisections (Fig. 1, E and F): postp3 invariably developed as a slightly shortened d3, whereas most antp3 were transformed to a d2 identity (83%, $n = 58$). Transformations of identity were restricted to manipulated primordia; anteriorization of digits did not cause processive anteriorization of identity along the A/P axis. The expression of *Hox*D10-12, previously suggested to have a role in patterning the digital arch (*9*), was unaffected by the transformations of identity (*7*) ($n > 5$ for each gene). When p3 were bisected at later stages, approximately when the first interphalangeal joint is being specified (Fig. 1G), antp3 developed with a chimeric d2/d3 morphology (67%, $n = 6$). Later stage p3 bisections (Fig. 1H) resulted in both postp3 and antp3 developing as d3 (100%, $n = 8$). Combined, these data demonstrate that A/P identity is not a stable property of condensing digital primordia, but progressively becomes fixed along the proximodistal axis as outgrowth occurs and molecular positional information is translated into morphological form.

The interdigits (IDs) are wedges of mesoderm separating digital primordia of the developing autopod (Fig. 1B). Following proximodistal specification of the limb, ID mesoderm undergoes apoptosis and regresses, correlating with the free digits of amniotes such as chickens and humans (*10*). ID tissue has not been implicated in patterning the autopodial skeleton. We performed two sets of experiments to assess if digital primordia receive A/P positional instruction from ID mesoderm. First, p2 and p3 were bisected, and the posterior components, along with their associated IDs, were removed (Fig. 2A). The isolated antp2 and antp3 were transformed to d1 (Fig. 2B) and d2 (Fig. 2C), respectively, in 90% of specimens ($n = 22$ for p3, $n = 10$ for p2), confirming the results of the foil

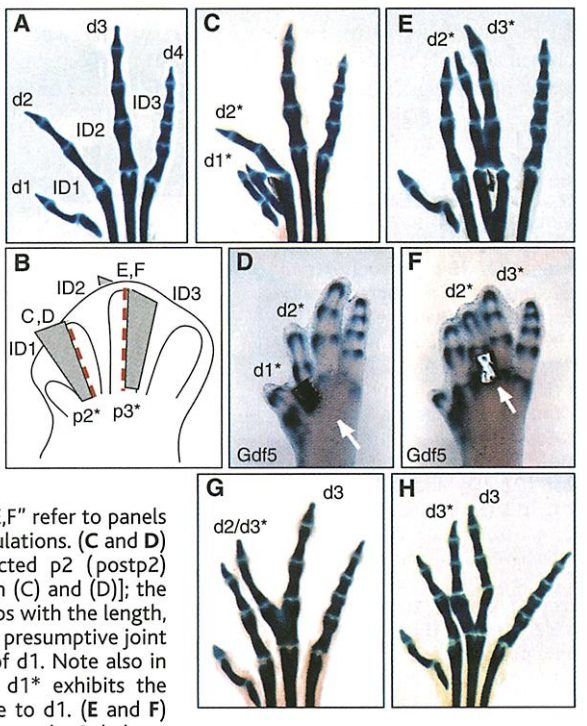

Fig. 1. A/P identity is not a fixed property of digital primordia. In all panels, developing feet are shown in dorsal view with posterior to the right, anterior to the left. (A, C, E, G, and H) HH St. 36 feet (*6*) stained with Victoria blue to reveal cartilage patterns. (D and F) HH St. 32 whole-mount in situ hybridization with *Gdf5* to visualize presumptive joints. (**A**) Control limb with labeled digits (d1 through d4) and interdigital regions (ID1 through ID3). Note that d4 has five phalanges, d3 has four, d2 has three, and d1 has two. (**B**) Surgical schematic depicting the bisection (dashed red lines) of digit 2 and 3 primordia (p2* and p3*, respectively) and insertion of foil barriers (gray wedges); "C,D" and "E,F" refer to panels showing the results of these manipulations. (**C** and **D**) The posterior component of bisected p2 (postp2) develops as a normal digit 2 [d2* in (C) and (D)]; the anterior component (antp2) develops with the length, phalangeal number [d1* in (C)], and presumptive joint pattern [d1* in (D)] characteristic of d1. Note also in (C) that the proximal phalanx of d1* exhibits the distinctive ventral concavity unique to d1. (**E** and **F**) The respective components of bisected p3 behave similarly, with postp3 developing as d3 (d3*) and antp3 adopting a d2 identity (d2*). Digital identity becomes progressively fixed; d3 bisection at the time the metatarsophalangeal joint forms results in antp3 developing with chimeric d2/d3 identity (**G**), whereas subsequent bisections result in antp3 developing with invariant d3 identity (**H**). Control bisections of d2 and d3, with no further manipulation, had no effect ($n = 46$). In (D) and (F), foil barriers are indicated by white arrows. For additional technical comments on all experiments in this report, see (*11*).

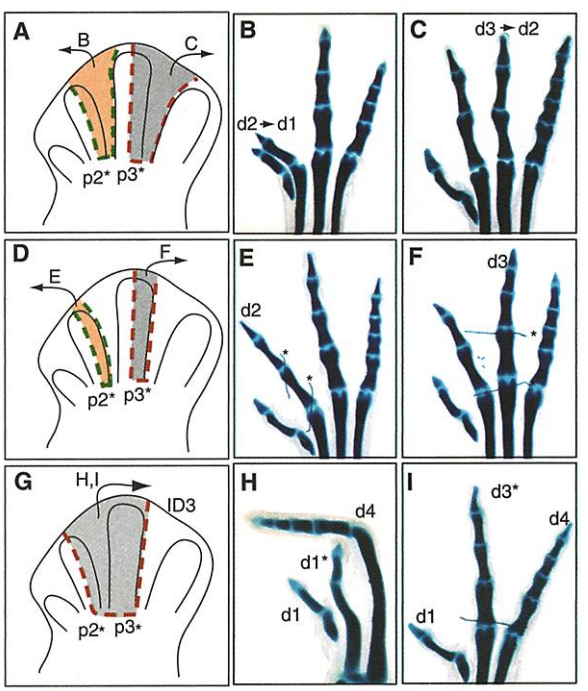

Fig. 2. A/P positional value resides in the ID mesoderm. (**A**) Schematic removal of postp2 and postp3, plus the associated ID2 and ID3, respectively (orange with green dashed line, B; gray with red dashed line, C). The remaining antp2 and antp3 develop as homeotically transformed d1 (**B**) and d2 (**C**). (**D**) Surgical protocol in which only postp2 (**E**) and postp3 (**F**) were excised and wound surfaces joined with pins [black asterisks in (E) and (F)]. Reestablished contact between antp2 and ID2 restores d2 identity (E), whereas antp3/ID3 rejuxtaposition restores d3 identity (F). The collective removal of postp2, ID2, and p3 (**G**) results in antp2 developing as d1 [d1* in (**H**)]; this result is similar to (B), but with the additional deletion of the third digit and metatarsal. Antp2 pinned to ID3 (**I**) develops as d3 (d3*).

barrier experiments above. Similar experiments on p3 of the wing resulted in antp3 developing as d2 (*11*). Second, we removed only the posterior components of bisected primordia and reestablished contact between anterior components and the ID lying posteriorly by pinning (Fig. 2D). In these experiments, normal digital identity was restored in 100% of cases (Fig. 2, E and F; $n > 10$ for each). Further, if antp2 is apposed to ID3, it develops as d3 (Fig. 2I) instead of d1 (Fig. 2H), representing a posteriorization of two digital positions (78%, $n = 9$). These observations support a three-part model: A/P positional information downstream of the ZPA is retained in the ID mesoderm, which in turn specifies digital identity; more posterior IDs specify more posterior digital identities (e.g., ID3 specifies d3, ID2 specifies d2, and so forth); and digital identity is determined by the posteriormost ID cue a primordium receives (e.g., ID3 cues supersede ID2 or ID1 instruction in specifying d3 identity).

The results of other manipulations support this model. The removal of complete IDs (Fig. 3A) caused anterior transformations. Excision of ID2 (Fig. 3B) resulted in p2 developing as d1 (43%, $n = 7$), while removal of ID3 (Fig. 3C) caused p3 to develop as d2 (41%, $n = 22$). Transformations were never observed in digits posterior to excised IDs. Further, "isotopic" grafts of donor p2 into host ID2 (Fig. 3D) and donor p3 into host ID3 (Fig. 3E) invariably developed with d2 and d3 identity, respectively ($n > 6$ for each). In contrast, p3 grafted into the more anterior ID2 (Fig. 3F) developed as d2 (75%, $n = 8$), whereas p2 grafted into ID3 (Fig. 3G) were posteriorly transformed to d3 (24%, $n = 21$). A model in which digital precursors arise with an anterior identity and are promoted to more posterior identities in a stepwise fashion (*4*) cannot account for anterior digital transformations. It is notable that our combined embryological data do not support this hypothesis.

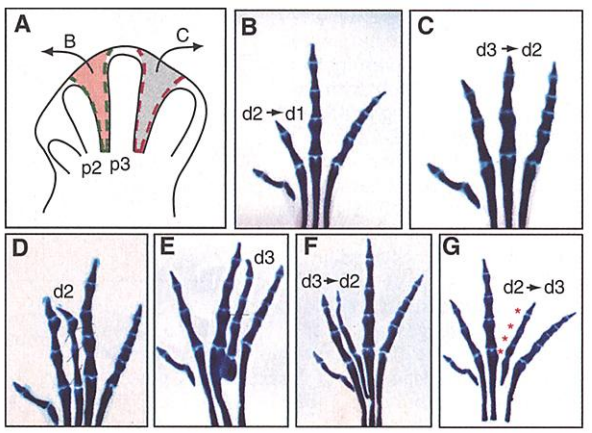

Fig. 3. Interdigits specify digital identity. (**A**) ID2 (orange; B) and ID3 (gray; C) removals. In the absence of ID2 instruction, p2 develops as a characteristically shortened, biphalangeal d1 (**B**); likewise, ID3 removal effects the transformation of d3 to d2 (**C**). In (D) through (G), donor digital primordia were grafted into heterotopic host ID environments. Control grafts of donor p2 to host ID2 (**D**) and donor p3 to host ID3 (**E**) invariably result in normal d2 and d3 development, respectively. In contrast, grafts of p3 to a more anterior host ID2 position causes transformation to d2 identity (**F**), whereas the more posterior host ID3 environment imposes a more posterior d3 identity on grafted p2 (**G**). Joint planes are indicated by red asterisks in (G).

We next investigated which ID signaling molecules mediate the transfer of A/P positional information to digital primordia. SHH-N–loaded beads implanted in ID3 caused the flanking p3 and p4 primordia to develop with an additional phalanx (Fig. 4A; 72%, $n = 47$); we interpret these to be posterior transformations of identity. SHH-N application to each ID demonstrated that all primordia were posteriorly respecified (Fig. 4B) with similar frequency (83%, $n = 23$). It is unlikely that SHH-N acts directly on primordia to posteriorize digital identity, as SHH-N beads induced expression of the SHH-responsive genes *Ptc* (*12*) and *Hip* (*13*) throughout ID mesoderm, but not in flanking primordia (*7*). Rather, our data suggest that SHH-N treatment augments ID signaling pathways that normally act during development to specify posterior digital identities.

The BMP family of signaling molecules are candidates for regulating digital identity. *Bmp2*, *Bmp4*, and *Bmp7* are expressed by the IDs during the developmental time (*14*) in which we have determined digital identity is specified. Addition of BMP2-expressing cells to early limb buds can posteriorize induced supernumerary digits (*4*), while misexpression of the constitutively active BMP type 1 receptor *BmpR1b* in mouse hind limb mesenchyme causes the anteriormost d1 to develop as d2 (*15*). We found that ID application of SHH-N caused the upregulation of *Bmp2*, *Bmp4*, and *Bmp7* (Fig. 4C) (*7*), as well as *BmpR1b* (Fig. 4D), supporting assertions that increased levels of BMP signaling specifies more posterior digital identity (*4, 15*). Moreover, we confirmed that increased levels of ID BMPs are necessary for posterior respecification of digital fate: coadministration of beads treated with SHH-N and the BMP antagonist Noggin (Fig. 4E), which binds BMP2, BMP4, and BMP7 and blocks activation of BMP receptors (*16*), abrogates SHH-N–mediated posterior transformations [94%, $n = 17$ ($P < 0.01$)].

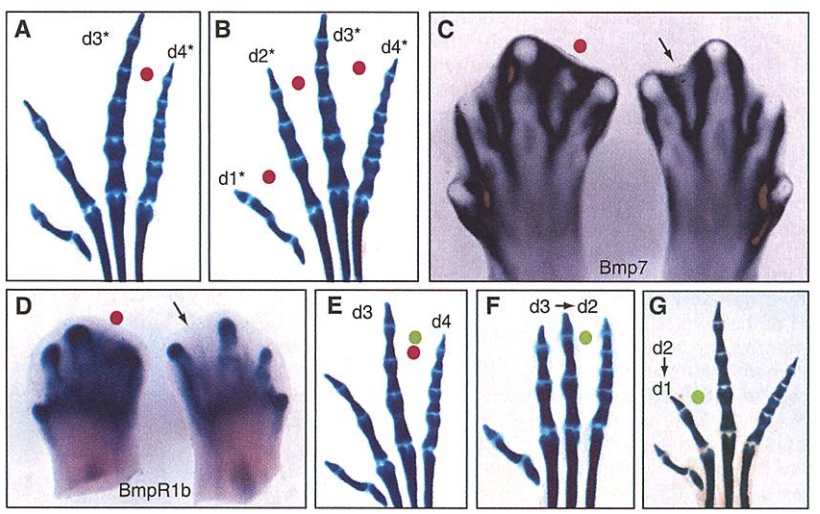

Fig. 4. Modulation of ID BMP levels causes homeotic digital transformation. (**A**) Application of SHH-N–soaked beads (red circles) to host ID3 causes incomplete posterior transformations of identity in the flanking d3 and d4 positions. The five phalanges in the d3 position (d3*) are characteristic of d4 identity, although digit length and phalangeal morphology are incompletely transformed. The six phalanges of the d4 position represent a neomorphic transformation to a novel digital structure (d4*). (**B**) SHH-N application to each ID causes each digit to develop with an additional phalanx. Ectopic *Bmp7* (**C**) and *BmpR1b* (**D**) expression in SHH-N–treated ID3s correlates with posterior transformations of identity. In (C) and (D), contralateral control limbs are shown in reversed A/P orientation on the right in order to compare treated (red circles) with untreated (arrows) ID3s. (**E**) Coimplantation of beads loaded with SHH-N and the BMP antagonist Noggin (green circles) restores normal digital development. Application of Noggin-soaked beads to host ID3 (**F**) and ID2 (**G**) causes anterior transformations of digital identity. Control beads did not affect cartilage patterning ($n = 68$).

Attempts to posteriorize digital identity by enhancing ID BMP levels with exogenous BMP2 and BMP4 were unsuccessful. BMP2- and BMP4-loaded beads were implanted in ID2 and ID3, over a wide range of concentrations and developmental time (*11*). In agreement with previous reports (*17, 18*), we observed combinations of truncations, joint deletions, and cartilage dysmorphologies (96%, $n = 160$) that precluded assessment of digit respecification. However, several developing tissues exhibit markedly different responses to treatment with specific combinations of homo- and heterodimeric BMP ligands (*19–21*). Thus, although application of homodimeric BMP2 and BMP4 can only elicit the above dysmorphologies, we agree with the recently proposed possibility that other combinatorial repertoires of homo- and heterodimeric BMP ligands may regulate digital identity (*4*) during normal development.

As an alternative approach, we assessed the effects of reduced ID BMP levels. Noggin-loaded beads applied to ID3 (Fig. 4F) and ID2 (Fig. 4G) caused the transformation of d3 to d2 (23%, $n = 48$) and d2 to d1 (21%, $n = 14$), respectively. Noggin-mediated transformations correlated with reduced ID *Bmp2*, *Bmp4*, and *Bmp7* expression, whereas *Hox*D10-12 expression was not affected [$n > 10$ for each probe (*7*)], further suggesting that the *Hox*D complex does not play a primary role in establishing digit identity. These results confirm previously reported *Bmp4*, *Hox*D11, and *Hox*D13 expression in the IDs of chick leg buds with inhibited BMP signaling due to ectopic expression of a dominant negative *BmpR1b* receptor (dn*BmpR1b*) (*22*). Interestingly, figure 1B of (*22*) shows a dn*BmpR1b*-expressing foot with apparent anterior transformations of digital identity (*23*).

Combined with, and in the context of, our embryological and molecular analyses, published data can be interpreted to suggest that experimental modulation of ID BMP signaling can cause both anterior and posterior transformations of digit identity, with higher BMP levels necessary (*22*) and sufficient (*4, 15*) for the development of more posterior identities. Therefore, it is of interest that Noggin-mediated inhibition of mandibular arch BMP signaling causes homeotic transformations of tooth identity (*24*). We suggest that differential BMP signaling may represent a conserved mechanism for specifying discrete identities among meristic structures within a developmental field.

Our results indicate that A/P identity is not an inherent property of digital primordia, but is specified by the ID mesoderm prior to its regression. We show that more posterior IDs specify more posterior digital identities, and that digital fate is determined by the most posterior ID cues a primordium receives. We further demonstrate that digit identity can be transformed through experimental modulation of ID BMP signaling, suggesting the BMP family plays a role in regulating digital identity. These data represent an important advance in understanding how autopodial mesoderm organizes A/P positional information downstream of ZPA signaling and directs the skeletal patterning of the digital arch [for a schematic model, see (*11*)]. By extension, this study highlights the importance of understanding the intermediary molecular mechanisms that convert early ZPA signals into the interdigitally compartmentalized arrangement of A/P positional information present at later stages.

References and Notes

1. R. L. Johnson and C. J. Tabin, *Cell* **90**, 979 (1997).
2. R. V. Pearse and C. J. Tabin, *J. Exp. Zool.* **282**, 677 (1998).
3. Y. Yang *et al.*, *Development* **124**, 4393 (1997).
4. G. Drossopoulou *et al.*, *Development* **127**, 1337 (2000).
5. E. E. Storm and D. M. Kingsley, *Development* **122**, 3969 (1996).
6. V. Hamburger and H. L. Hamilton, *J. Morphol.* **88**, 49 (1951).
7. R. D. Dahn and J. F. Fallon, data not shown.
8. W. Bateson, *Materials for the Study of Variation, Treated with Especial Regard to Discontinuity in the Origin of Species* (MacMillan and Co., London, 1894).
9. J. Zákány and D. Duboule, *Cell Tissue Res.* **296**, 19 (1999).
10. J. W. Saunders Jr. and J. F. Fallon, *Major Problems in Developmental Biology* (Academic Press, New York, 1967), pp. 289–314.
11. Supplemental technical comments and data are available at www.sciencemag.org/feature/data/1049492.shl
12. V. Marigo, M. P. Scott, R. L. Johnson, L. V. Goodrich, C. J. Tabin, *Development* **122**, 1225 (1996).
13. P. T. Chuang and A. P. McMahon, *Nature* **397**, 617 (1999).
14. E. Laufer, S. Pizette, H. Zou, O. E. Orozco, L. Niswander, *Science* **278**, 305 (1997).
15. Z. Zhang *et al.*, *Dev. Biol.* **220**, 154 (2000).
16. L. B. Zimmerman, J. M. DeJesús-Escobar, R. M. Harland, *Cell* **86**, 599 (1996).
17. Y. Gañan, D. Macias, M. Duterque-Coquilluad, M. A. Ros, J. M. Hurle, *Development* **122**, 2349 (1996).
18. D. Macias *et al.*, *Development* **124**, 1109 (1997).
19. A. Aono *et al.*, *Biochem. Biophys. Res. Commun.* **210**, 670 (1995).
20. A. Suzuki, E. Kaneko, J. Maeda, N. Ueno, *Biochem. Biophys. Res. Commun.* **232**, 153 (1997).
21. S. Nishimatsu and G. Thomsen, *Mech. Dev.* **74**, 75 (1998).
22. H. Zou and L. Niswander, *Science* **272**, 738 (1996).
23. Figure 4B of Zou and Niswander (*22*) shows the cartilage pattern of a dn*BmpR1b*-expressing chick foot relative to the unmanipulated control foot. In the normal foot, d4 has five phalanges and d3 has four. In the infected foot, d4 appears to have four phalanges, whereas d3 appears to have three. Zou and Niswander suggest that dn*BmpR1b* expression causes distally incomplete digits to develop; however, these digits exhibit perfectly formed distal claws. Alternatively, we interpret this phenotype as dn*BmpR1b*-mediated digital fate transformations (d4 to d3 and d3 to d2) due to inhibited ID BMP signaling.
24. A. S. Tucker, K. L. Matthews, P. T. Sharpe, *Science* **282**, 1136 (1998).

25. We thank C. Tabin, J. Hurle, D. Kingsley, L. Niswander, R. Harland, W. Smith, A. McMahon, and Genetics Institute, Inc. for providing reagents; C. Tabin, S. Carroll, G. Panganiban, D. Stocum, and Fallon lab members for suggestions; S&R Egg Farm (Whitewater, WI) for providing the White Leghorn flock. R.D.D. acknowledges J. George, L. Saucedo, and F. Zappa. This work was funded by NIH grant HD32551 to J.F.F. and an NSF Predoctoral Fellowship, NIH Training Grant #T32HD07477, and a Kremer Fellowship to R.D.D.

15 February 2000; accepted 1 June 2000

Evidence for Ecological Causation of Sexual Dimorphism in a Hummingbird

Ethan J. Temeles,* Irvin L. Pan, Jillian L. Brennan, Jedediah N. Horwitt

Unambiguous examples of ecological causes of animal sexual dimorphism are rare. Here we present evidence for ecological causation of sexual dimorphism in the bill morphology of a hummingbird, the purple-throated carib. This hummingbird is the sole pollinator of two *Heliconia* species whose flowers correspond to the bills of either males or females. Each sex feeds most quickly at the flower species approximating its bill dimensions, which supports the hypothesis that floral specialization has driven the evolution of bill dimorphism. Further evidence for ecological causation of sexual dimorphism was provided by a geographic replacement of one *Heliconia* species by the other and the subsequent development of a floral dimorphism, with one floral morph matching the bills of males and the other of females.

Sexual dimorphism in size and morphology is widespread in animals. Charles Darwin drew attention to these differences and offered three explanations for their evolution that were based on mechanisms of sexual selection, fecundity selection, and ecological causation (for example, resource partitioning) (*1*). Although empirical studies have demonstrated that the first two mechanisms operate in natural populations (*2*), unambiguous examples of ecological causation of sexual dimorphism are absent from the literature, an exception being some mosquito species, in which the mouthparts of males are adapted for drinking nectar and the mouthparts